Taylor & Francis
Taylor & Francis Group

∂ OPEN ACCESS | Check for updates

Functional amyloid protein FXR1 is recruited into neuronal stress granules

Anna A. Valina [a,b], Tatyana A. Belashova [a,c], Anastasia K. Yuzman[b], Sergey P. Zadorsky [a,b], Evgeniy I. Sysoev [a,b], Vladimir A. Mitkevich [d], Alexander A. Makarov [d], and Alexey P. Galkin [a,b]

aSt. Petersburg Branch, Vavilov Institute of General Genetics, Russian Academy of Sciences, St. Petersburg, Russian Federation; bDepartment of Genetics and Biotechnology, Faculty of Biology, St. Petersburg State University, St. Petersburg, Russian Federation; cLaboratory of Amyloid Biology, St. Petersburg State University, St. Petersburg, Russian Federation; dEngelhardt Institute of Molecular Biology, Russian Academy of Sciences, Moscow, Russian Federation

ABSTRACT

The FXR1 protein regulates the stability and translation of a number of RNA molecules and plays an important role in the regulation of cellular processes under normal conditions and stress. In particular, this protein is known to be a negative regulator of the key proinflammatory cytokine TNF alpha. We had previously shown that FXR1 functioned in the amyloid form in neurons of the brain of jawed vertebrates. Under stress conditions, FXR1 is incorporated into stress granules in some cell lines, but such studies have not been conducted for neuronal cells. Here, we showed the ability of the FXR1 protein to form cytoplasmic granules in a neuroblastoma cell line under various types of stress. This protein colocalizes with core proteins of neuronal stress granules upon heat shock and sodium arsenite treatment. We also showed that FXR1 colocalizes with anti-amyloid antibodies OC under both normal and stress conditions. Given that stress granules are dynamic structures, we propose that amyloid FXR1-containing RNP particles interact with other stress granule proteins through weak intermolecular hydrogen bonds. Using a yeast model system, we found that FXR1 colocalizes and physically interacts with stress granule proteins such as TIA-1, FMRP, FXR2, and SFPQ. Overall, our results provide new insights into the role of the RNA-binding protein FXR1 in neuronal stress response. We believe that FXR1 inactivation in neuronal stress granules can contribute to an increase in the level of the proinflammatory cytokine TNF alpha in neurodegenerative diseases.

Introduction

In cells, messenger RNA (mRNA) is never alone but is always covered by RNA-binding proteins (RBPs) which can alter the fate or function of the bound mRNA thereby modulating gene expression [1]. RBPs, in turn, may be compacted into large ribonucleoprotein (RNP) granules or assemblies – membrane-less organelles that form through multivalent RNA–RNA, RNA–protein and protein–protein interactions [2]. RBPs are known to modify the output of post-transcriptional and epigenetic gene expression throughout the entire life cycle of mRNA: transcription, 5′ end capping, precursor mRNA splicing, 3′ end processing, nuclear export, localization, translation, and mRNA stability [3]. These functions of RBPs are carried out by binding to sequence and/or structural motifs in RNA via modular combinations of globular RNA-binding domains (RBDs) such as RNA recognition motif (RRM), hnRNP K homology domain (KH) [4] or DEAD box helicase domain [5] along with non-canonical RBDs [6].

Currently, over 1500 RBPs have been discovered throughout the human genome, accounting for ~7.5% of protein-coding genes. However, only a few of them have been functionally described [7]. Among the described RBPs with canonical RBDs, the FXR1 protein is present [8]. The domain structure of FXR1 includes classical RBDs such as two KH motifs and three arginine-rich regions (RG, RGG, R) [9]. Besides this, FXR1 contains two Tudor domains and a coiled-coil domain (also known as the KH0 domain) which mediate dimerization and other protein–protein interactions [10,11]. Such multidomain structure of FXR1 determines its multifunctionality in regulating the fate of transcripts. Thus, the participation of the FXR1 protein in such processes of RNA metabolism as miRNA processing [12], regulation of localization [13], stability [14], translation [15], and RNA editing [16] is known.

The FXR1 protein belongs to a family of structurally very similar RBPs, highly homologous FXR proteins.

FXR genes family includes Fragile X mental retardation 1 (*FMR1*) encoding the FMRP protein, *FMR1* autosomal homolog 1 (*FXR1*) and *FMR1* autosomal homolog 2 (*FXR2*) genes which have been identified on human chromosomes Xq27.3, 3q26.33, and 17p13.1, respectively [17]. The percentage of identical amino acid residues between the sequences of FMRP, FXR1 and FXR2 proteins is approximately 60%. Homology is particularly observed in the first 13 of 17 exons, for which the amino acid sequence identity is 73–90% [18]. Despite high homology, the expression levels of *FMR1*, *FXR1* and *FXR2* are different and tissue-specific [19–21]. However, all three genes show similarly high levels of expression in differentiated neurons of the adult brain. In the adult cerebellum, the strongest expression of *FMR1*, *FXR1* and *FXR2* was observed in the cytoplasm of neurons and especially Purkinje cells [22]. FMRP, FXR1 and FXR2 play different roles in embryogenesis and postnatal development as the corresponding knockout mice exhibit different phenotypes [23]. This could be explained by the fact that FXR proteins target different mRNAs [17]. The main targets of FXR1 binding are AU-rich elements located in the 3'-untranslated region of many mRNAs with a short half-life. In particular, FXR1 has been shown to be a negative regulator of the key proinflammatory cytokine Tumor Necrosis Factor alpha (TNFα) [14,24].

All three proteins of FXR family, like many other RBPs, are known to be found in stress granules (SGs) [25] – membrane-less transient RNP assemblies that form in the cytoplasm of cell as a result of protein/RNA phase separation in response to exposure to various environmental stressors and facilitate the majority of cell types to survive [26]. SG assembly is accompanied by translational repression and disassembly of translating polysomes [2]. The rapid emergence of SGs may occur through a pre-existing network of SG protein interactions in non-stressed cells that facilitates rapid fusion into larger SGs [25]. SGs are transient assemblies comprised a stable core substructure that is surrounded by a more dynamic shell, wherein the components are in a dynamic equilibrium with polysomes [27]. Core components of SGs, including nucleating Ras GTPase-activating protein-binding protein 1 (G3BP1), T-cell intracellular antigen-1 (TIA-1), TIA-1-related (TIAR) protein, tristetraprolin (TTP), and FMRP, initiate the SG formation process by binding to each other, as well as to polyadenylated mRNA and 40S ribosomal subunits. In the next step, SG nucleators induce homotypic and heterotypic interactions between other SG proteins, resulting in the maturation of SGs [28]. The composition of dynamic SGs depends on the cellular

and environmental context [25,29]. Interestingly, neuronal cells display a greater diversity in SG composition compared to non-neuronal cells. Many of the components of such neuronal SGs have been reported to function in protein quality control pathways, potentially providing an explanation to why neurons are especially vulnerable to environmental stresses [25].

The formation of SGs, causing reprogramming of the translation, is observed in neurodegenerative diseases such as amyotrophic lateral sclerosis, Huntington's disease, Alzheimer's disease (AD), multiple sclerosis, and frontotemporal dementia [25,30]. The formation of persistent SGs and the aberrant localization of Splicing factor, proline- and glutamine-rich (SFPQ) and tau proteins in them correlate with the rapid progression of AD [31]. It should also be noted that the level of TNFα, which is negatively regulated by FXR1, significantly increases during neurodegenerative inflammation [32].

In this regard, it seems very intriguing that one of the SG proteins, the FXR1 protein, normally, without any stress, is present in amyloid form in the cytoplasm of neurons in the brain of various vertebrate species [33,34]. We had previously shown that FXR1 clearly colocalized in cortical neurons with the amyloid-specific dyes Congo red (CR), Thioflavins S and T. FXR1 fibrils extracted from the brain by immunoprecipitation showed yellow-green birefringence after staining with CR which definitely proves the amyloid nature of this protein. Moreover, FXR1 had been shown to perform its molecular RNA-binding function in the amyloid conformation: RNA molecules colocalized with FXR1 in cortical neurons were insensitive to treatment with RNase A [33]. However, the possible incorporation of FXR1-containing amyloid particles into neuronal SGs has not been studied. Here, we analyse the ability of the FXR1 protein to form cytoplasmic granules and its colocalization with SG core proteins in human neuroblastoma cells in response to various stress stimuli. We also study the physical interaction of FXR1 with individual SG proteins in a yeast-based system. Overall, our results indicate that functional amyloids may play an important role in regulating the neuronal stress response.

Results

FXR1 is recruited to cytoplasmic granules in stressed SH-SY5Y cells

To address the question of whether FXR1 forms cytoplasmic stress-induced granules in neuronal cells, we first analysed its localization in the human SH-SY5Y

neuroblastoma cell line exposed to different stressors. We tested the effect of acute inflammation, serum starvation, oxidative stress and heat shock. The cells grown on glass coverslips were maintained at 37°C (control) or subjected to stress listed above and then immediately fixed in paraformaldehyde (PFA).

Neither acute inflammation induced by 1300 ng/ml of TNFα for 1 h (Figure 1b) nor serum starvation for 24 h (Figure 1c) resulted in the formation of FXR1-containing granules in SH-SY5Y cells. No cytological differences were observed compared to control cells (Figure 1a). In contrast, cells treated with 3 mm sodium arsenite (SA) for 1 h or heat-treated at 43°C for 30 min (heat shock) showed numerous cytoplasmic granules visible under a light microscope (Figure 1d, e).

The FXR1 protein is a component of stress granules in SH-SY5Y neuroblastoma cell line

Sodium arsenite and heat shock are well-known inducers of SGs. However, to date, there is no convincing evidence that these treatments actually lead to incorporation of FXR1 into the neuronal SGs. So far, such experiments have been performed on non-neuronal cell lines [35–37].

To understand whether the FXR1-containing granules found in SH-SY5Y cells are SGs, we performed double immunofluorescence assays with antibodies to FXR1 and one of the core SG proteins (FMRP or TIA-1). In this case, TIA-1 acts as an excellent marker for SG formation, since in response to stress, TIA-1 translocates from the nucleus (its subcellular localization in normal conditions) to the cytoplasm and is subsequently incorporated into large SGs.

As before, neuroblastoma SH-SY5Y cells were subjected to SA (3 mm, 1 h) and heat shock (43°C, 30 min). In control cells, immunofluorescent staining with anti-FXR1 and anti-FMRP antibodies revealed, as expected, a cytoplasmic localization both FXR1 and FMRP with a small number of little granules (Figure 2a). Both oxidative and heat stresses resulted in the formation of FXR1-containing SGs in SH-SY5Y
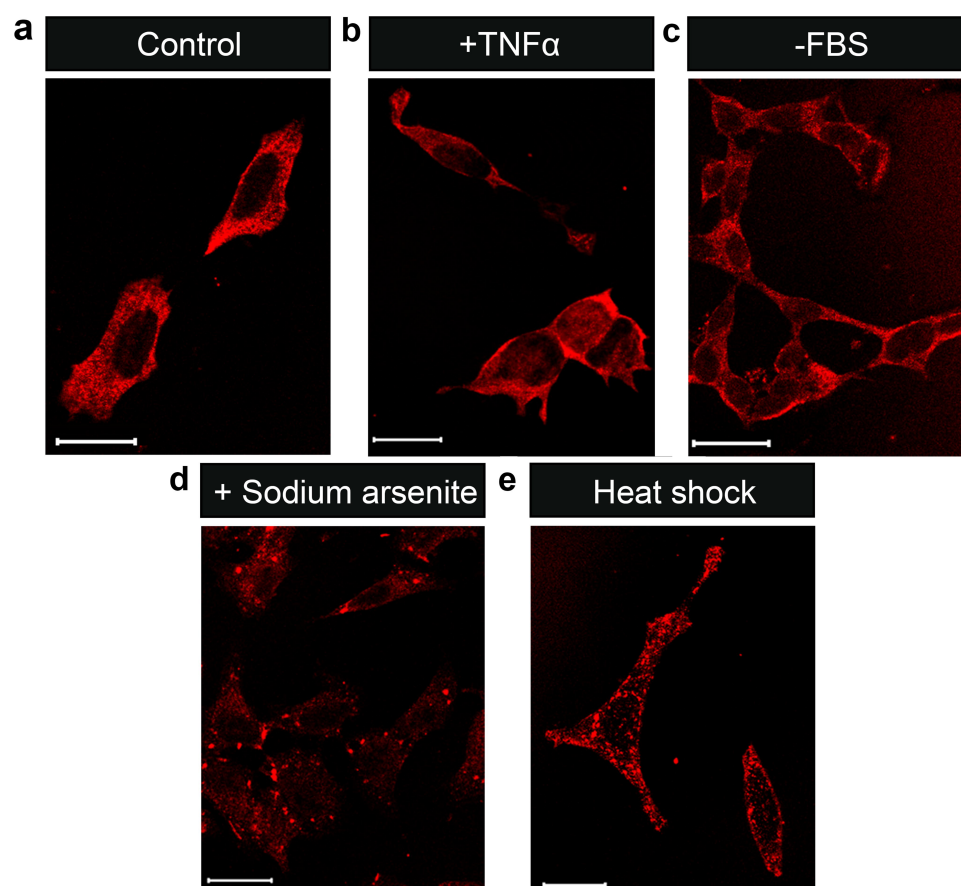
Figure 1. FXR1 form numerous large cytoplasmic granules under sodium arsenite and heat shock treatment but not under acute inflammation and serum starvation in SH-SY5Y cells. SH-SY5Y cells were cultured at normal conditions (a), treated with 1300 ng/ml of TNFα for 1 h (b) or subjected to serum starvation for 24 h (-FBS) (c). SH-SY5Y cells were treated with 3 mm SA for 1 h (d) or cultured at 43°C for 30 min (e). Cells were subsequently fixed, permeabilized, and analysed by immunofluorescence with antibodies against the FXR1 protein (ab51970, Abcam) (red fluorescence). Scale bars, 20 μm.

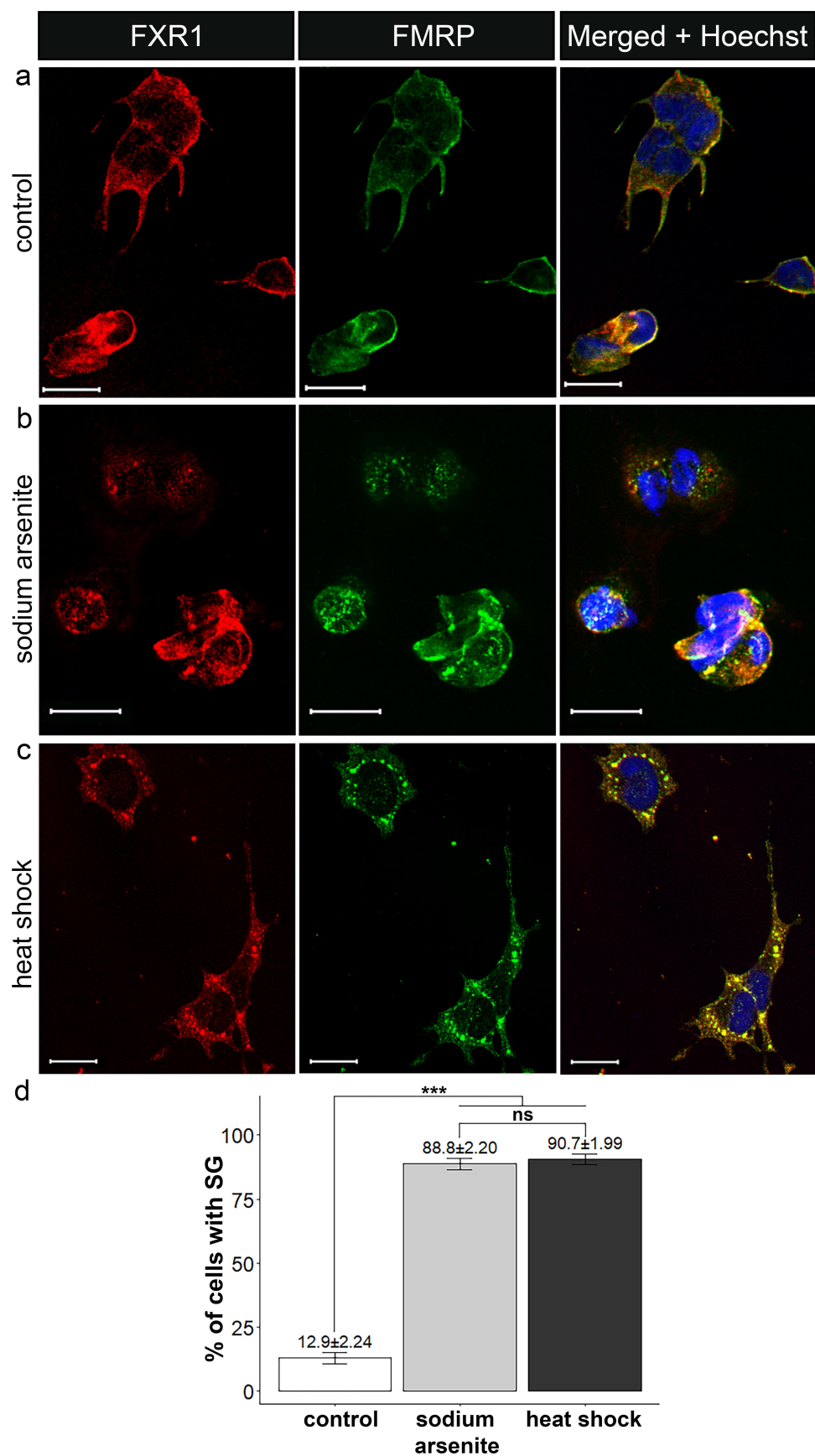**Figure 2.** FXR1 is recruited to FMRP-positive stress granules upon sodium arsenite and heat shock treatment in SH-SY5Y cells. SH-SY5Y cells were cultured at normal conditions (a) or were treated for 1 h with 3 mm SA (b) or for 30 min at 43°C (c). Cells were subsequently fixed, permeabilized, and analysed by immunofluorescence with antibodies against FXR1 (ab51970, Abcam) (red

cells as evidenced by apparent colocalization with another SG-associated protein FMRP (Figure 2b, c). The reliability of SG formation under used stress conditions is confirmed by the fact that the number of FMRP-positive SGs induced by both stress treatments was statistically significant greater compared to control ($p < 0.05$) (Figure 2d, Supplementary Table S1).

The observed incorporation of FXR1 into SGs of SH-SY5Y was supported by immunofluorescent staining with anti-FXR1 and anti-TIA-1 antibodies. In control cells FXR1 demonstrate cytoplasmic localization (Figure 3a), while the TIA-1 protein is characterized by nuclear localization (Figure 3a). Under both oxidative stress and heat shock, TIA-1 partially relocates from the nucleus to cytoplasm, and large TIA-1-positive SGs appear. These TIA-1-containing SGs clearly colocalize with the FXR1 protein (Figure 3b, c).

Protein extract immunoprecipitated by anti-FXR1 antibodies from neuroblastoma cells contains amyloid fibrils

We had previously shown that the FXR1 protein is presented in amyloid form in the cytoplasm of cortical neurons of various vertebrate species [33,34]. In this study, we asked whether the amyloid conformation of FXR1 is preserved when it is incorporated into SGs. To study this issue, we compared the localization of antibodies to FXR1 and Anti-Amyloid Fibrils OC antibodies on fixed SH-SY5Y cells in normal and stress conditions. OC antibodies recognize generic epitopes common to many amyloid fibrils and fibrillar oligomers [38]. FXR1 colocalizes with anti-amyloid antibodies OC under both normal and stress conditions (Figure 4). However, colocalization with OC antibodies does not prove that exactly FXR1 is the amyloid component of SGs. To test this hypothesis, we isolated FXR1 by immunoprecipitation from cell culture exposed and unexposed to SA. We had previously shown that FXR1 is present in the form of amyloid fibrils in the cytoplasm of rat brain neurons [33]. The fibrillar structures are detected by transmission electron microscopy (TEM) in both stressed and unstressed cells (Figure 5a, b). Single fibrils are combined into large bundles. This is likely due to the process of concentration of these fibrils by ultracentrifugation after immunoprecipitation with anti-FXR1 antibodies. As shown

in Figure 5b, the fibrils isolated from cells exposed to SA are associated with proteins that do not have a fibrillar structure. It can be assumed that these are SG proteins associated with FXR1 fibrils. The immunoprecipitated fibrils from SH-SY5Y cells bind CR and exhibit apple-green birefringence under crossed polarized light (Figure 5c, d). These results suggest that FXR1 is included in the composition of SG in the form of amyloid particles.

FXR1 fused to a fluorescent protein interacts with the SG proteins in a yeast model

We have shown that FXR1 is a component of SGs, but these data do not allow us to conclude that FXR1 physically interacts with the SG proteins. It is known that the formation of SG is determined by RNA-protein and protein–protein interactions [39]. Protein–protein interactions in SGs are almost unstudied, since SGs contain many proteins, and it is impossible to evaluate individual interactions in mammalian cell culture. In this regard, we assessed the colocalization and physical interaction of FXR1 with some SG proteins in a yeast model system.

We cotransformed yeast cells with the following pairwise plasmid combinations: FXR1-CFP and YFP-FMRP, FXR1-CFP and YFP-FXR2, FXR1-YFP and TIA-1-CFP, or FXR1-CFP and SFPQ-YFP (experimental combinations); and FXR1-YFP and PrP-CFP (negative control combination). PrP-CFP aggregates in yeast cells [40] but is not predicted to interact with any of the SG proteins. PrP in neurons and neuroblastoma cells is a receptor and is localized on the surface of the cell membrane [41,42]. This protein has recently been shown to colocalize with SGs in HeLa cells [43], but most likely this is a specific feature of HeLa cells.

In this work, we used truncated sequences of the $FMRP_{1-380}$ and $FXR2_{14-399}$ proteins, corresponding to two Tudor domains, the KH0 domain, and two RNA-binding KH motifs. Since the key role of the KH0 domain in protein–protein interactions of FXR family proteins has been established [10], it is assumed that truncated versions of the FMRP and FXR2 proteins are sufficient for studying their protein–protein interactions with the FXR1 protein in a yeast model. Yeast cotransformants were analysed by confocal laser-scanning microscopy (Figure 6a).

---

fluorescence) and FMRP (ab17722, Abcam) (green fluorescence) proteins. Nuclei were stained with Hoechst 33342 (blue fluorescence). Scale bars, 20 µm. (d) The fraction of cells with FMRP-positive SGs was quantified (~200 cells per condition, *** – $p \leq 0.05$, ns – $p > 0.05$). Standard error of percentage is indicated as error bars. Chi-Square test was performed to compare frequencies of cells with SGs.
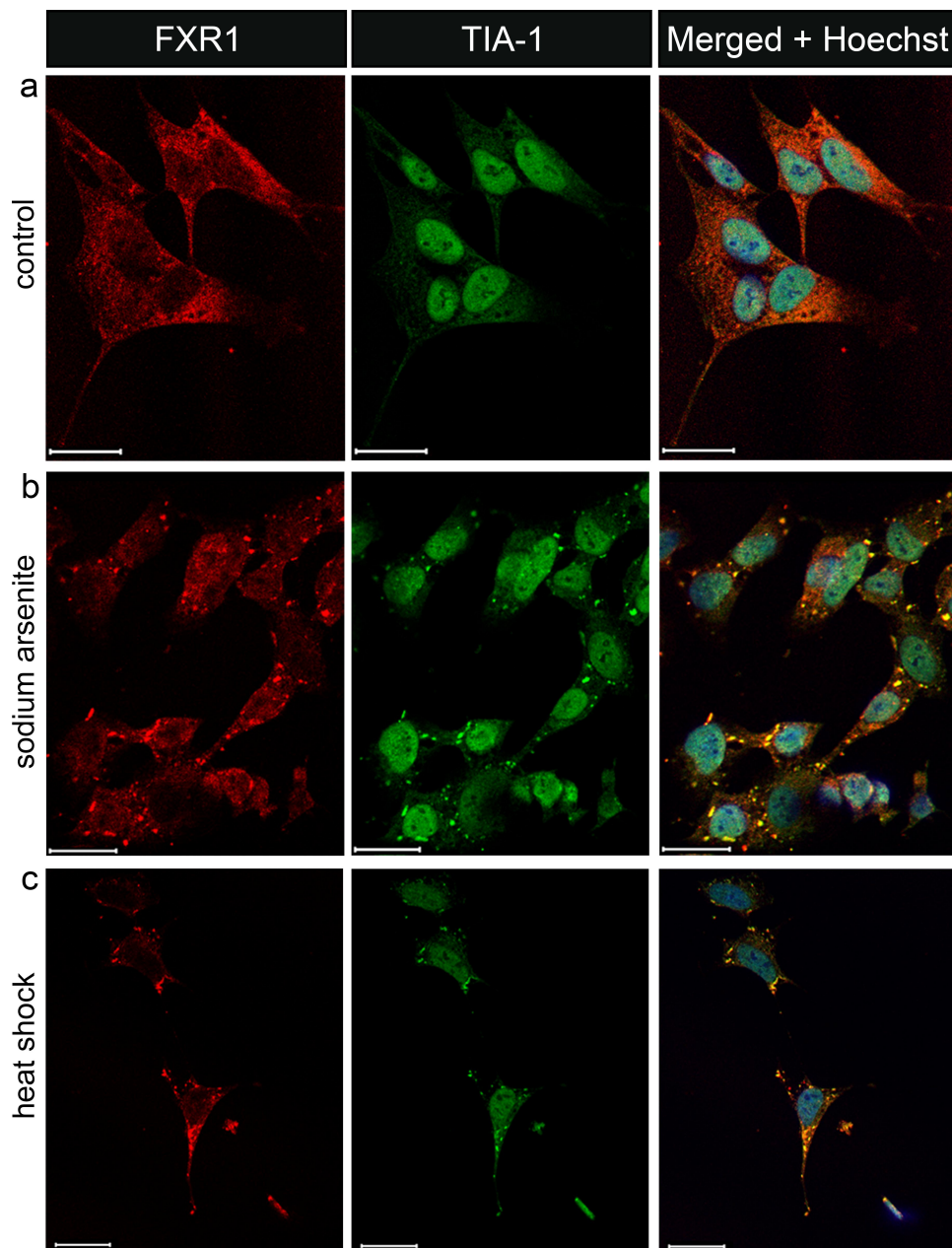
Figure 3. FXR1 is recruited to TIA-1-positive stress granules upon sodium arsenite and heat shock treatment in SH-SY5Y cells. SH-SY5Y cells were cultured at normal conditions (a) or were treated for 1 h with 3 mm SA (b) or for 30 min at 43°C (c). Cells were subsequently fixed, permeabilized, and analysed by immunofluorescence with antibodies against FXR1 (ab51970, Abcam) (red fluorescence) and TIA-1 (K109466P, Solarbio) (green fluorescence) proteins. Nuclei were stained with Hoechst 33342 (blue fluorescence). Scale bars, 20 μm.

The analysis of yeast cells containing microscopically detectable FXR1 aggregates revealed colocalization of the fluorescent signals between FXR1 and all analysed SG proteins (Figure 6a). The colocalization frequencies were 94.4%, 80.0% and 73.3% for core SG proteins $FMRP_{1-380}$, TIA-1 and $FXR2_{14-399}$, respectively (Figure 6b). In the yeast cells producing FXR1-CFP and facultative SG protein SFPQ fused with YFP, fluorescent signals colocalized with a frequency of 45.0%. The colocalization frequencies of all experimental combinations were statistically significant greater ($p < 0.05$) than negative control frequency of FXR1 and PrP colocalization (20.0%) (Figure 6b, Supplementary Table S2). The low frequencies of colocalization of FXR1-YFP and PrP-CFP can be explained by non-specific binding of proteins that form aggregates in yeast cells.

To analyse possible physical interaction of the SG proteins in yeast cells, we applied the FRET method [44] which is based on energy transfer between a donor (CFP fusion protein) and an acceptor (YFP fusion
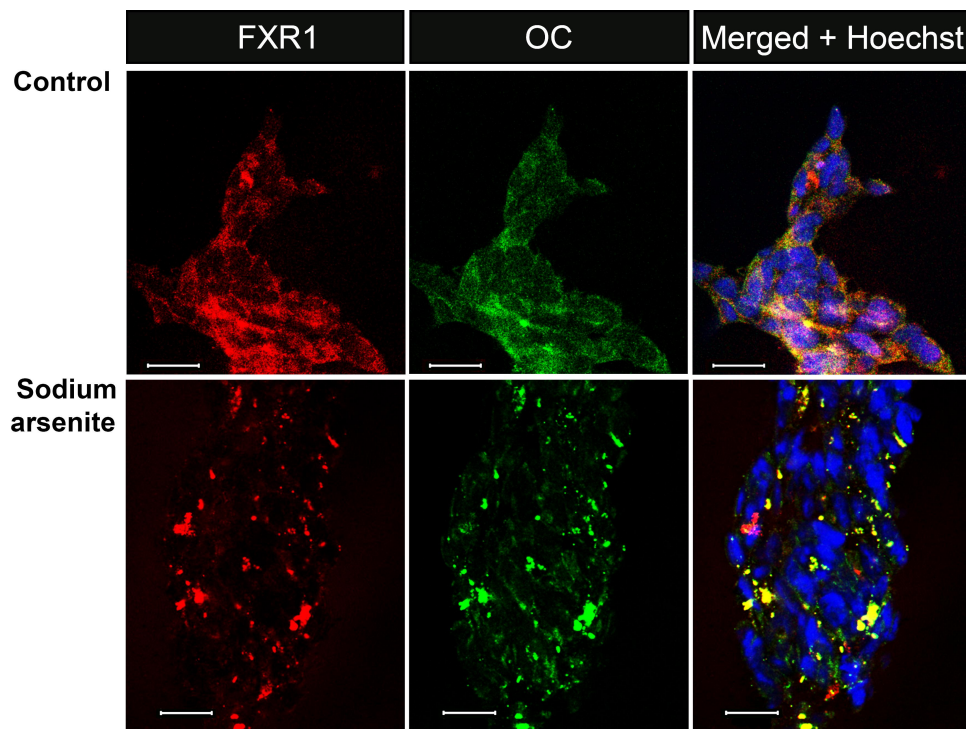
Figure 4. FXR1 colocalizes with anti-amyloid antibodies OC under both normal and stress conditions. The cells were cultured at normal conditions (control) or were treated for 1 h with 3 mm SA, subsequently fixed, permeabilized, and analysed by immunofluorescence with antibodies against FXR1 (ab51970, Abcam) (red fluorescence) and Anti-Amyloid Fibrils OC antibodies (AB2286, Sigma-Aldrich) (green fluorescence). Nuclei were stained with Hoechst 33342 (blue fluorescence). Scale bars, 20 μm.
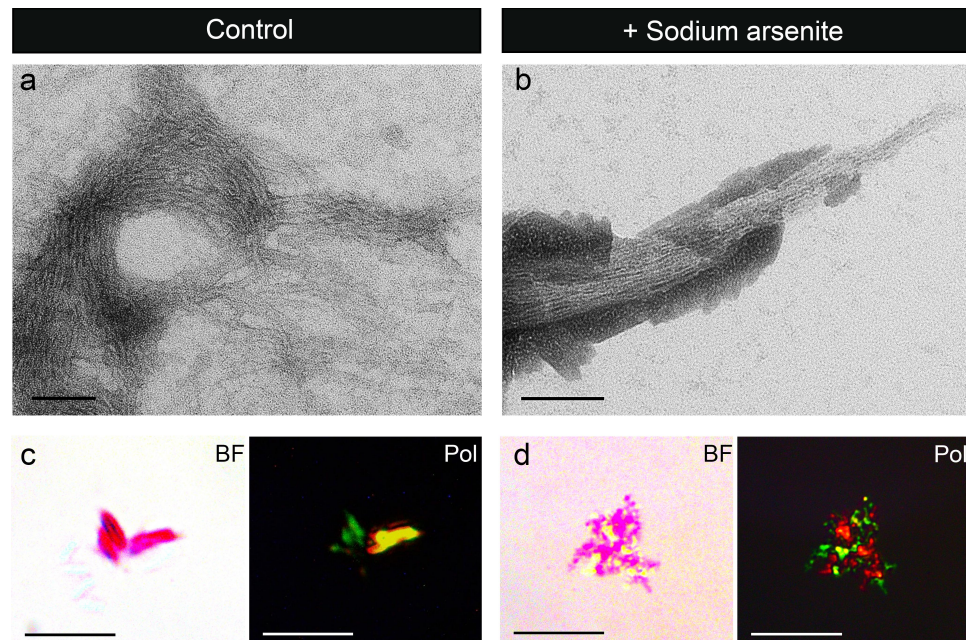

Figure 5. Fibrils immunoprecipitated with polyclonal anti-FXR1 antibodies from the SH-SY5Y cells at normal conditions and under sodium arsenite treatment. Electron micrographs of fibrils stained with uranyl acetate from unstressed (a) and stressed neuroblastoma cells (b). CR staining of the protein immunoprecipitated from unstressed (c) and stressed neuroblastoma cells (d). The left panels are brightfield (BF), and the right panels are polarized light (Pol). Scale bars, 100 nm (a, b); 20 μm (c, d).
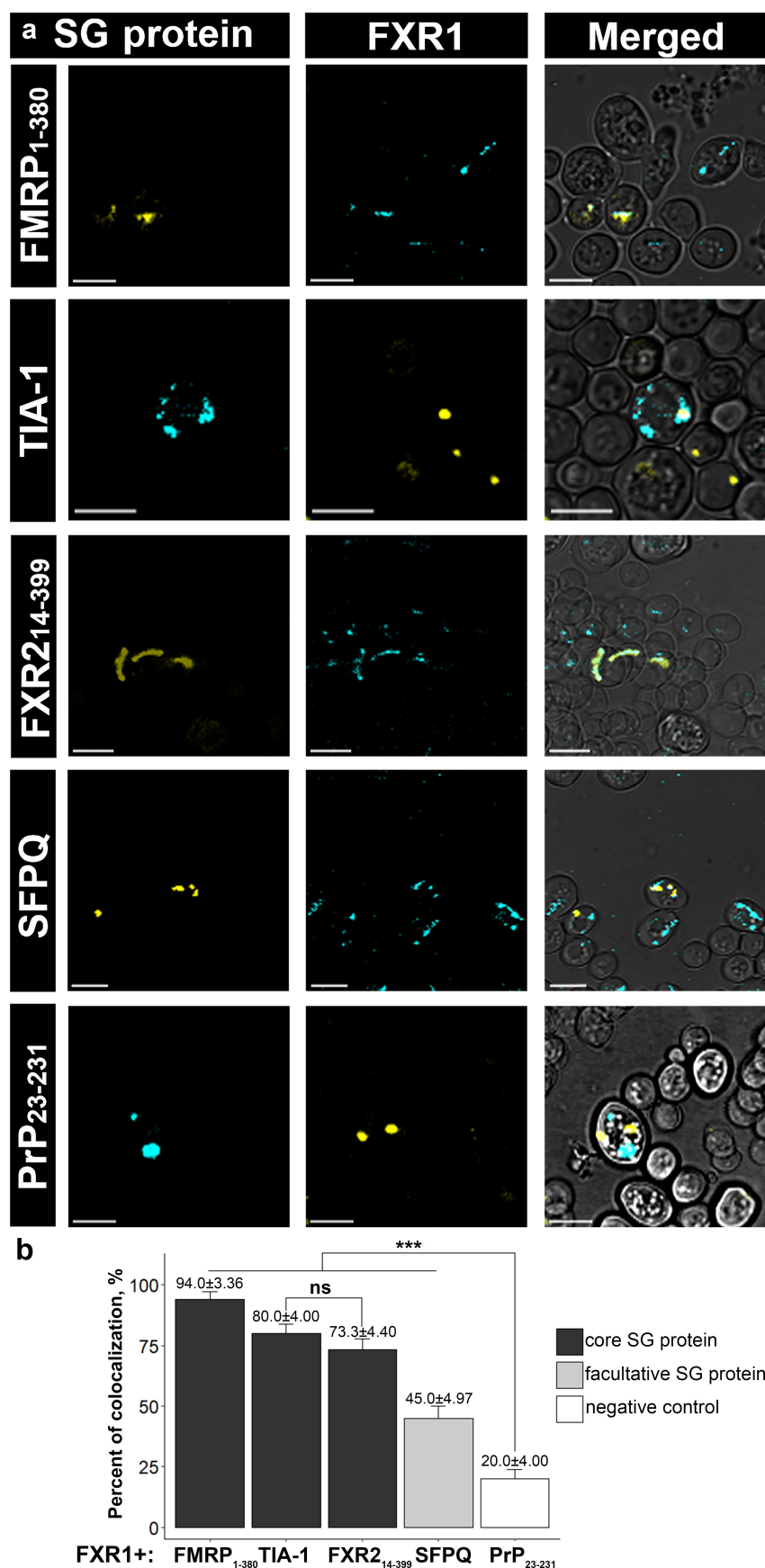
Figure 6. FXR1 colocalizes with other SG proteins (FMRP$_{1-380}$, TIA-1, FXR2$_{14-399}$, and SFPQ) in a yeast model. (a) Confocal laser-scanning microscopy of yeast cells co-expressing FXR1 and other SG proteins. Scale bars, 5 μm. (b) The colocalization frequencies between FXR1 aggregates and one of the SG proteins in yeast. At least 50 cells per combination, *** – $p \leq 0.05$, ns – $p > 0.05$. Standard error of percentage is indicated as error bars. Fisher's exact test was performed to compare colocalization frequencies. n = 3 per protein combination.

protein) molecule at short distances (up to 10 nm) [45]. We measured the efficiency of energy transfer (FRET$_{eff}$) by comparing the donor fluorescence intensity before and after acceptor photobleaching. The FRET$_{eff}$ value was measured for three independent biological replicates for each plasmid combination given above. In this experiment, FXR1-CFP and FXR1-YFP protein combination acted as a positive control for protein interaction. The pair FXR1-CFP and YFP, which does not interact with FXR1, was used as a negative control combination.

The degree of interaction of homoprotein combination (FXR1-CFP and FXR1-YFP) was 8.9% efficiency of FRET. The negative control combination of FXR1-CFP with the YFP protein showed only about 3%. Corresponding values of FRET$_{eff}$ were accepted as standards of presence and absence of physical interaction of proteins in yeast cells, respectively. In combinations of FXR1 with all analysed SG proteins, a FRET efficiency was not statistically different from the positive control and was statistically different ($p < 0.05$) from the negative control (Figure 7). The corresponding values of FRET$_{eff}$ were 9.7%, 8.3%, 5.9%, and 9.1% for FMRP$_{1-380}$, FXR2$_{14-399}$, TIA-1, and SFPQ, respectively (Figure 7). This indicates the presence of a physical interaction between FXR1 and all SG proteins analysed, which confirms the results of colocalization of FXR1 with FMRP and TIA-1 obtained in the SH-SY5Y neuroblastoma cell line (Figures 2,3).

Discussion

In a neuronal cell model, the SH-SY5Y cell line, we showed that sodium arsenite treatment and heat shock result in the incorporation of the FXR1 protein into SGs containing the core SG proteins FMRP and TIA-1. Moreover, the observed cytological findings were supported by analysing the physical interactions between FXR1 and other SG proteins, FMRP, FXR2, TIA-1, and SFPQ, using the FRET method in a yeast model.

Immunocytochemical and immunoprecipitation assays show that neuronal SG contain amyloid inclusions (Figures 4,5). It has previously been shown that short motifs of SG proteins such as FUS, TDP-43, hnRNPA1 and mutant TIA-1 form a cross-β spine of amyloid fibrils [46–50], but in vivo, these proteins do not form amyloid structures. Our data support the hypothesis that RNA-binding protein FXR1 is incorporated into SG in amyloid form. We cannot completely exclude that colocalization with amyloid-specific antibodies and detection of amyloid fibrils after immunoprecipitation both under normal and stress conditions are explained by the interaction of FXR1 with some other amyloid protein. However, considering that FXR1 was previously detected in amyloid form in neurons of the vertebrate brain [33], such a suggestion seems unlikely. At the same time, it is not at all necessary that the mechanism of inclusion of FXR1 in the stable SG core involves amyloid interactions. Although SGs are
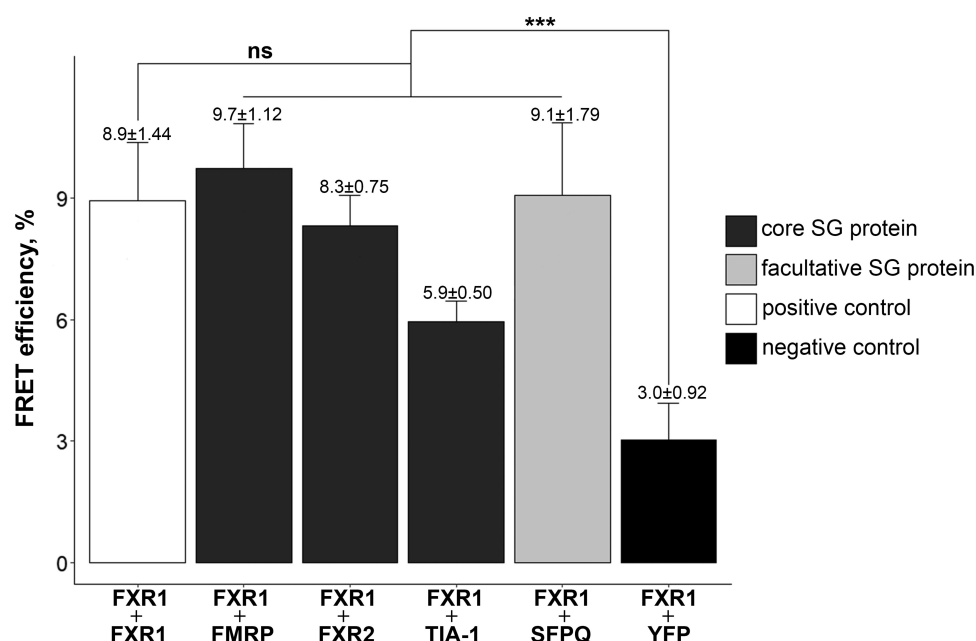

Figure 7. FXR1 physically interacts with other SG proteins (FMRP$_{1-380}$, FXR2$_{14-399}$, TIA-1, and SFPQ) in a yeast model. FRET efficiency values for the following protein combination is presented: FXR1-CFP + FXR1-YFP, FXR1-CFP + FMRP$_{1-380}$-YFP, FXR1-CFP + FXR2$_{14-399}$-YFP, FXR1-YFP + TIA-1-CFP, FXR1-CFP + SFPQ-YFP, and FXR1-YFP + PrP$_{23-231}$-CFP. At least 50 cells per protein combination, *** − $p \leq$ 0.05, ns − $p > 0.05$. Standard error of mean is indicated as error bars. Student's t-test was performed to compare FRET efficiency values. n = 3 per protein combination.

dynamic structures, it is difficult to imagine that their disassembly involves the disassembly of amyloid fibrils, which are characterized by high stability and resistance to various physicochemical factors [51]. Moreover, post-translational modifications that do not affect the amyloidogenic domain may be responsible for the inclusion of FXR1 in SGs.

Although there was no previous cytological evidence for FXR1 incorporation into neuronal SGs, this protein was identified in the screening of G3BP1-positive SGs from neural progenitor cells derived from human-induced pluripotent stem cells [25]. This work also revealed that all FXR proteins, together with another core SG protein TIA-1, interact with G3BP1 in the absence of stress, suggesting a pre-existing network of protein interactions that likely facilitates the rapid coalescence of SGs under stress [25]. This assumption is confirmed by the results of our analysis of the efficiency of physical interaction of SG proteins using the FRET method in yeast cells. According to the obtained $FRET_{eff}$ values (Figure 7), corresponding to the efficiency of energy transfer between the analysed protein pair, the strength of interaction of FXR1 with SG proteins decreases in the following order: FMRP (9.7%), SFPQ (9.1%), FXR2 (8.3%), and TIA-1 (5.9%). It is not surprising that the affinity of FXR1 for other members of FXR protein family is somewhat higher than for core SG protein TIA-1, since the analysed truncated versions of the $FMRP_{1-380}$ and $FXR2_{14-399}$ proteins contained a coiled coil (the KH0 domain) that is known to mediate protein–protein interaction among the FXR proteins. It is worth noting that this motif is coded for by exon 7 which is one of the most highly conserved regions among members of the FXR family in divergent organisms [10]. Although it was unexpected to find a high $FRET_{eff}$ value for the pair FXR1 and SFPQ, it can be assumed that the presence of a coiled coil domain in the composition of SFPQ [52] is responsible for this interaction. It is possible that FXR1 physically interacts with SFPQ less frequently than with the core SG proteins, but this FXR1-SFPQ interaction appears to be relatively stable.

Finally, a logical question arises: what could be the consequences of the inclusion of FXR1 in neuronal SGs? Since the molecular functions of FXR1 as an RBP are very diverse, the fate of the transcripts bound by it may vary. Translocating into the SGs, FXR1 brings there the mRNA, thereby repressing its overall translation and downregulating the expression of the corresponding gene. On the other hand, the incorporation of FXR1, which acts as an RNA destabilizing protein, in the SGs may lead to the removal of the existing repression block of some mRNA, since newly synthesized transcripts will

not bind to FXR1 and, therefore, can avoid a decay. This is particularly interesting for inflammatory mRNAs, whose stability is reduced by FXR1 [14]. Among the proinflammatory targets of FXR1, transcripts of IL-1β, ICAM1, CCL2 and TNFα were found. It has been also demonstrated that knock down of FXR1 leads to increasing in the stability of these transcripts [14]. It can be assumed that the incorporation of FXR1 into SGs may lead to increased production of proinflammatory cytokines. This statement seems especially important in the context of neurodegenerative inflammation which is accompanied by the appearance of persistent SGs.

Overall, the obtained data support our hypothesis that amyloid particles of FXR1 are a component of neuronal SGs. These data may be important for understanding the structural organization of neuronal SGs and their role in activating translation of proinflammatory cytokines in neurodegenerative diseases.

Materials and methods

Cell lines, culture conditions, and stress induction

The SH-SY5Y cell line used in this study is a subclone derived from the human neuroblastoma cancer cell line SK-N-SH. SH-SY5Y cells were generously provided by Evgeniy V. Kanov, Institute of Translational Biomedicine, St. Petersburg State University, St. Petersburg, Russia. The cell line was maintained in DMEM/F12 (Biolot, 1.3.7.4.) supplemented with 10% fetal bovine serum (FBS; HyClone (Cytiva), SV30160.03) and antibiotics (100 units/ml penicillin, 100 μg/ml streptomycin; Gibco, 15140122) at 37°C in a humidified incubator with 5% CO_2. Cells were treated with 3 mm of sodium arsenite (Sigma-Aldrich, S7400) for 1 h to induce oxidative stress and SG formation. To induce heat shock, SH-SY5Y cells were maintained at 43°C for 30 min. Starvation was modelled by maintaining neuroblastoma cells in DMEM/F12 supplemented with antibiotics (100 units/ml penicillin, 100 μg/ml streptomycin) without the addition of FBS for 24 h. Acute inflammation was simulated by treating the cells with 1300 ng/ml of TNFα (SCI-store, #PSG250) for 1 h. All stress treatments were performed when cells reached 75–80% confluency.

Antibodies

Commercially available primary antibodies against the following antigens were used: FXR1: goat polyclonal, ab51970 (Abcam), or rabbit polyclonal, DF12402 (Affinity Biosciences); FMRP: rabbit polyclonal, ab17722 (Abcam); TIA-1: rabbit polyclonal, K109466P

(Solarbio). Rabbit Anti-Amyloid Fibrils OC antibodies (AB2286) were obtained from Sigma-Aldrich. Donkey anti-Goat IgG (H+L) secondary antibodies coupled with Alexa Fluor 647 (A32849) and goat anti-Rabbit IgG (H+L) secondary antibodies coupled with Alexa Fluor 488 (A32731) were obtained from Invitrogen.

Immunofluorescence microscopy of SH-SY5Y cells

SH-SY5Y cells grown to confluency on glass coverslips were exposed to stress as described above and then fixed with 4% PFA (Sigma-Aldrich, 158127) for 10 min at room temperature (RT). The cells were subsequently permeabilized with 0.1% Triton X-100 (Sigma-Aldrich, T8787)/phosphate-buffered saline (PBS) for 1 h at RT and washed three times with 0.1% Tween-20 (Sigma-Aldrich, P1379)/PBS (PBS-t). For the blocking step, 1% human serum albumin (HSA; Sigma-Aldrich, A3782)/PBS-t was used for 1 h at 37°C. For immunofluorescence analysis of FXR1 localization, coverslips were incubated with anti-FXR1 primary antibodies diluted in PBS-t (1/100) overnight at 4°C. For double-staining immunofluorescent studies, coverslips were incubated with a pair of primary antibodies (FXR1+TIA-1, FXR1 +FMRP, FXR1+OC) diluted in PBS-t overnight at 4°C. The antibodies dilutions were 1/100, 1/300, 1/300, and 1/750 for anti-FXR1, anti-FMRP, anti-TIA-1, and anti-Amyloid fibrils (OC), respectively. The coverslips were then washed three times with PBS-t and incubated with Alexa Fluor 488 goat anti-rabbit IgG (1/500) and Alexa Fluor 647 donkey anti-goat IgG (1/500) for 1 h at RT. After five washes with PBS-t, Hoechst 33342 Ready Flow Reagent (Invitrogen, R37165) was applied at a dilution of 1/300 for 7 min to stain nuclei. Fluorescence microscopy was performed using a TCS SP5 confocal laser-scanning microscope (Leica Microsystems) and Leica Application Suite X 3.3.0.16799 software. Images were compiled using Adobe Photoshop v. 22.0.1 software.

Analysis of amyloid properties of the FXR1 protein ex vivo

A comparative analysis of the amyloid properties of the FXR1 protein in SH-SY5Y cells under normal and stress conditions was performed using the amyloid fibril immunoprecipitation approach [33]. Preparation of cell lysates for immunoprecipitation was performed by homogenization of unstressed and stressed SH-SY5Y cells with glass beads in lysing buffer (50 mm Tris-HCl, pH 7.6, 150 mm NaCl, 1 mm EDTA, 2 mm PMSF, 1 mm DTT, 1 × Halt™ Protease Inhibitor Cocktail (Thermo Fisher Scientific, 78429)) using a FastPrep24 benchtop homogenizer (MP Biomedicals). The used parameters were 6.0 m/s for 20 sec with incubation on ice for at least 3 min. The procedure was repeated five times. Normalization to the total protein in the obtained lysates was performed using the Qubit method. For immunoprecipitation of the FXR1 protein from neuroblastoma cells, the anti-FXR1 primary antibodies (Affinity Biosciences, DF12402) were bound with the protein A-coated magnetic bead SileksMag-Protein A (Sileks, K0181) in binding buffer (PBS, 0.02% Tween-20 (Sigma-Aldrich, P1379), 1 × Halt™ Protease Inhibitor Cocktail (Thermo Fisher Scientific, 78429), 2 mm PMSF) for 1 h at RT with slow overhead rotation. The prepared magnetic beads with antibodies were then incubated with lysate from the unstressed and stressed cells overnight at 4°C. Protein elution was performed with 125 mM glycine buffer (pH 2.1) for 10 min at RT according to the manufacturer's protocol. After neutralization by 1.5 M Tris-buffer (pH 8.8), the fibrils were sedimented by centrifugation at 436,000 g for 2 h at 4°C, analysed by TEM or stained with CR dye followed by analysis in brightfield and polarization light.

Sample preparation for TEM and fibril structure analysis

Negatively stained samples were prepared on a formvar-coated copper grid (Formvar/Carbon Film 10 nm/1 nm thick on Square 300 mesh Copper Grid; Electron Microscopy Sciences, FCF300-Cu-50). A 10 µL aliquot of the fibril solution was adsorbed to the formvar grid for 1 min, blotted, and then stained with 10 µL of 1% uranyl acetate (Electron Microscopy Sciences, 22400) for 1 min. After the removal of uranyl acetate, the probes were dried in the air. The fibril structure was analysed using a JEM-2100 hC electron microscope (JEOL). Adobe Photoshop v. 22.0.1 software was used for figure assembling.

Congo red staining of fibrils

A 10 µL aliquot of the fibril solution was put onto a glass microscope slide, air dried, stained with 50 µL of a 1% aqueous solution of CR (Sigma-Aldrich, C6767) for 5 min at RT, washed with water, and covered with a clean coverslip. Slides were analysed in brightfield and between cross polarizers on the microscope Biolar PI-PZO (PZO Microscopy).

Statistical analysis of SG formation

Cells with two or more large visible SGs stained with anti-FMRP antibodies were considered SG-positive cells. The number of SG-positive cells and the total number of cells per field of view (×40 magnification) were counted in six or more randomly selected fields of coverslip. For each type of stress exposure and under normal conditions, the total number of cells counted was more than 200. Statistical comparison between groups was performed by comparing the percentage of SG-positive cells from the total number of cells. To compare the frequencies of SG-positive cells, Chi-Square test was used, with $p \leq 0.05$. Statistical analyses and data visualization were performed using RStudio v. 2023.06.1 software. Bar charts represent percentage ± standard error of percentage.

Yeast and bacteria strains and growth conditions

To analyse FXR1 colocalization and physical interaction with SG-associated proteins, the yeast *S. cerevisiae* strain BY4742 (MATα his3Δ1 leu2Δ lys2Δ ura3Δ0) (Invitrogen) was used. Standard yeast genetic techniques, media, and cultivation conditions were used. Rich organic media (YEPD) and selective yeast minimal synthetic media (SD) were used for cultivation. To study the colocalization and physical interaction between proteins, yeast co-transformants were grown in a selective liquid medium lacking leucine and uracil for 2 days.

Yeast cells were grown in selective liquid media in the environmental shaking-incubator ES-20/60 (Biosan, Latvia) at 30°C, 200 rpm. About 100 μM copper sulphate ($CuSO_4$) (Sisco Research Laboratories, SRL-38869-500G) was added to a synthetic medium to induce gene expression under the *PCUP1* promoter. The *Escherichia coli* strain XL10-Gold (Tetr Δ (mcrA) 183, Δ (mcrBC-hsd SMR-mrr); Kan 173 endA1 sup E44 thi-1 recA1 gyrA96 relA1 lacHte [F' proAB lacIqZDM15 Tn10 (Tetr) Tn5 (Kanr) Amy]) (Stratagene, La Jolla, USA) was cultivated at 37°C in

Luria-Bertani agar plates containing ampicillin for propagation and selection of plasmids.

Cloning of the FMR1 and FXR2 genes

To construct plasmids with sequence encoding $FMRP_{1-380}$ and $FXR2_{14-399}$ fragments, coding sequence of the corresponding genes was obtained from cDNA of human neuroblastoma cells SH-SY5Y. At the first stage, SH-SY5Y cells were lysed using TRIzol reagent (Thermo Fisher Scientific, 15596026) according to the manufacturer's protocol, then total RNA was extracted using chloroform and isopropanol. cDNA synthesis using oligo(dT)12-18 was performed with SuperScript III Reverse Transcriptase (Thermo Fisher Scientific, 18080044) according to the manufacturer's protocol. cDNA was further used for *FMR1* and *FXR2* fragments amplification by PCR with Taq polymerase (ThermoFisher Scientific, EP0401) with the pair of primers encoding *Sfi*I restriction sites: FMR1_For_SfiI, FMR1_Rev_SfiI, and FXR2_For_SfiI, FXR2_Rev_SfiI, respectively (Table 1). The $FMR1_{1-380}$ and $FXR2_{14-399}$ genes were cloned into pJET 1.2 using a CloneJET PCR Cloning Kit (Thermo Fisher Scientific, K1231) according to the manufacturer's protocol.

Plasmids

All plasmids used in this study were multi-copy shuttle vectors with *URA3*, *LEU2* or *HIS3* markers that can propagate in *E. coli* and *S. cerevisiae* (all the plasmids are listed in Table 2).

The pRS415Cup-SFPQ-YFP(LEU2) plasmid was constructed by inserting PCR generated human *SFPQ* gene flanked with restriction sites *Hind*III and *Bam*HI into the pL-Cup1-YFP plasmid [53]. The sequence encoding human SFPQ was amplified by PCR from the Myc-Psf-WT plasmid (Addgene, #35183) using the primers SFPQ_For and SFPQ_Rev (Table 1).

To construct plasmids with sequence encoding $FMRP_{1-380}$ and $FXR2_{14-399}$ fragments, coding

Table 1. Primers used in the work.

Primer name	Sequence
SFPQ_For	5'-GTCAAGCTTATGTCTCGGGATCGGTTC-3'
SFPQ_Rev	5'-CCAGGATCCAAATCGGGGTTTTTTGTTTG-3'
FMR1_Rev_SfiI	5'-ATTGGCCGAGGCGGCCTCATGAAGCCACTAACACCCTCTG-3'
FMR1_For_SfiI	5'-ATTGGCCATTATGGCCGAGGAGCTGGTGGTGGAAGTG-3'
FXR2_For_SfiI	5'-ATTGGCCATTATGGCCCCCGTCGAGGTGCGCGGCTC-3'
FXR2_Rev_SfiI	5'-ATTGGCCGAGGCGGCCTCACCGCCCACTCCCAGGAGGGC-3'
FXR1_For	5'-TACAAGCTTATGGCGGAGCTGACGGT-3'
FXR1_Rev	5'-TACGGATCCATCACATCTTTTGCCTAGC-3'
CFP_For	5'-GGCGGATCCAGTAAAGGAGAAGAACTTTTCAC-3'
CFP_Rev	5'-GGCAGCGAGCTCTCATTTGTATAGTTCAT-3'
TIA1_For	5'-TTAAAGCTTATGGAGGACGAGATGCCCA-3'
TIA1_Rev	5'-TTAGGATCCCTGGGTTTCATACCCTGCCA-3'

Table 2. Plasmids used in the work.

Plasmid name	Yeast marker	Promoter/expression cassette
pRS415Cup-SFPQ-YFP(LEU2)	LEU2	pCup-SFPQ-YFP
pRS425Cup-YFP-FMRP$_{1-380}$ (LEU2)	LEU2	pCup-YFP-FMRP$_{1-380}$
pRS425Cup-YFP-FXR2$_{14-399}$ (LEU2)	LEU2	pCup-YFP-FXR2$_{14-399}$
pRS425Cup-FXR1-YFP(LEU2)	LEU2	pCup-FXR1-YFP
pRS316Cup-FXR1-CFP(URA3)	URA3	pCup-FXR1-CFP
pRS316Cup-TIA-1-CFP(URA3)	URA3	pCup-TIA-1-CFP
pRS316Cup-PrP$_{23-231}$-CFP(URA3)	URA3	pCup-PrP$_{23-231}$-CFP
pRS313Cup-YFP(HIS)	HIS3	pCup-YFP

sequence of the corresponding genes was obtained from cDNA of human neuroblastoma cells SH-SY5Y as described above. The fragments of *FMR1* and *FXR2* genes cloned into pJET 1.2 were digested with *Sfi*I restriction sites and inserted into the pRS425Cup-YFP-(LEU2) plasmid, which had been got from the plasmid pRS425:CUP-YFP-ctd (LEU2) plasmid (kindly provided by A.A. Rubel and A.A. Zelinsky, Laboratory of Amyloid Biology, St. Petersburg State University) by digestion with the same restriction sites. In this way, the final pRS425Cup-YFP-FMRP$_{1-380}$ (LEU2) and pRS425Cup-YFP-FXR2$_{14-399}$ (LEU2) plasmids were obtained.

The pRS316Cup-TIA-1-CFP(URA3) plasmid was constructed by two-step strategy. In the first step, the *Bam*HI-*YFP*-*Sac*I fragment of pU-Cup-YFP [53] was replaced with a PCR fragment encoding the cyan fluorescent protein (CFP) flanked with restriction sites *Bam*HI and *Sac*I. The coding sequence of CFP was PCR generated from the plasmid pDH5 (Addgene, #83775) using primers CFP_For and CFP_Rev (Table 1). The gained plasmid was named pU-Cup-CFP. At the second step, PCR generated sequence, encoding the human TIA-1 flanked with restriction sites *Hin*dIII and *Bam*HI, was inserted into pU-Cup1-CFP plasmid obtained in the previous step by digesting the vector with the same restriction sites. The *TIA-1* gene was amplified by PCR from the pET28a_TIA1 plasmid (Addgene, #106095) using the primers TIA1_For and TIA1_Rev presented in Table 1.

The pRS316Cup-FXR1-CFP(URA3) and pRS425Cup-FXR1-YFP(LEU2) plasmids were constructed by the following scheme: the sequence encoding human FXR1, flanked by the *Hin*dIII and *Bam*HI restriction sites, was amplified by PCR from the pFRT-TODestFLAGHAhFXR1 (Addgene, #48694) with FXR1_For and FXR1_Rev primers (Table 1). Thereafter, *FXR1* sequence was inserted in the pU-Cup-CFP (the construction is described above) and pL-Cup1-YFP (Antonets et al., 2016) plasmids digested with the same restriction sites [53].

The pRS316Cup-PrP$_{23-231}$-CFP(URA3) was constructed and described earlier by Rubel et al., 2013 [40]. The pRS313Cup-YFP(HIS) plasmid was kindly provided by A.A. Rubel and K.Y. Kulichikhin (Laboratory of Amyloid Biology, St. Petersburg State University).

Sanger sequencing was performed to validate the absence of significant mutations in any of the constructed plasmids. Yeast DNA transformations were performed by a protocol involving lithium acetate treatment and heat shock [54].

Fluorescence microscopy of yeast

The proteins studied in this work (FXR1, FXR2$_{14-399}$, FMRP$_{1-380}$, TIA-1, SFPQ, and PrP as a negative control) were fused to one of the fluorescent proteins (CFP or YFP). The TCS SP5 confocal laser-scanning microscope (Leica Microsystems Wetzlar GmbH) was used to examine FXR1 colocalization and the possibility of physical interaction with SG-associated proteins by the acceptor photobleaching FRET (AB FRET) method. Preliminary yeast cells were precipitated from the culture medium by centrifugation at 16,000 g, suspended in a drop of PBS and covered with a coverslip.

For excitation of fluorescent proteins, we used 458 nm and 514 nm argon lasers for the CFP fusion proteins and the YFP or YFP fusion proteins, respectively. The emission filters were 466 nm – 500 nm for the detection of CFP signals and 525 nm – 600 nm for the detection of YFP signals.

The FRET efficiency was measured as described previously by Rubel et al., 2013 [40,55], using Leica Application Suite X 3.3.0.16799 software (Leica Microsystems Wetzlar GmbH). In the FRET experiments CFP fusion proteins were a donor (Excitation (Ex) = 458 nm; Emission (Em) = 466–500 nm), while the YFP or YFP fusion proteins acted as an acceptor (Ex = 525 nm; Em = 600 nm). Acceptor photobleaching was performed using a 514 nm laser beam at 100% intensity.

Statistical analyses

To estimate colocalization frequencies between FXR1 and one of the SG-associated proteins (FXR2$_{14-399}$, FMRP$_{1-380}$, TIA-1 or SFPQ), we considered only cells with both CFP and YFP signals. Overall, more than 50 FXR1 aggregates were analysed. The colocalization frequencies (Cf) were measured as described previously by Sergeeva et al., 2018 [56]. To calculate Cf value for each pair of FXR1 with SG proteins, the following equation was used: $Cf = \frac{n*100\%}{N}$, where n – number of FXR1 aggregates that co-localize with another protein, N – total number of analysed FXR1 aggregates. Statistical analysis of FXR1 colocalization was performed using Fisher's exact test, with $p \leq 0.05$. Comparisons and data visualization were performed using RStudio v. 2023.06.1 software. Bar charts represent percentage ± standard error of percentage.

To calculate the effectiveness of the physical interaction between FXR1 and the SG proteins with the FRET method, the FRET efficiency (FRET$_{eff}$) parameter was used. FRET$_{eff}$ was measured by Leica LAS AF X 3.7.2.22383 software (Leica Microsystems GmBH, Germany), according to the following equation: $FRETeff = \frac{Dpost - Dpre}{Dpost}$, where Dpost is the donor fluorescence after photobleaching, and Dpre is the donor fluorescence before photobleaching.

In order to evaluate FRET efficiency, we calculated the average meaning of FRET$_{eff}$ in three independent cultures co-expressing FXR1 with different SG-associated proteins fused with CFP/YFP. As a negative control, we used a yeast strain co-producing the FXR1-CFP protein and a yellow fluorescent protein YFP. Yeast co-producing the FXR1-CFP and the FXR1-YFP was used as a positive control. For the statistical comparison of the FRET$_{eff}$, we used the Student's t-test with $p \leq 0.05$. Comparisons and data visualization were performed using RStudio v. 2023.06.1 software. Bar charts represent mean ± S. E.M., n corresponds to the number of biological replicates.

Author contribution

Conceptualization: A.P.G., A.A.V. Design of experiments: A. P.G., A.A.V., T.A.B., S.P.Z. Investigation: A.A.V., T.A.B., A.K. Y., S.P.Z, E.I.S., V.A.M. Statistical analysis: A.A.V. Writing – original draft preparation: A.A.V., A.K.Y. Writing – review and editing: A.P.G., E.I.S. Visualization: A.A.V., A.K.Y. Supervision, project administration, and funding acquisition: A.P.G., A.A.M. All authors have read and agreed to the published version of the manuscript.

Data availability statement

Data supporting the findings of this study are available from the corresponding author upon reasonable request.

Disclosure statement

No potential conflict of interest was reported by the author(s).

ORCID

Anna A. Valina http://orcid.org/0009-0004-8951-2295
Tatyana A. Belashova http://orcid.org/0000-0001-9433-6987
Sergey P. Zadorsky http://orcid.org/0000-0001-8859-164X
Evgeniy I. Sysoev http://orcid.org/0000-0003-1444-9784
Vladimir A. Mitkevich http://orcid.org/0000-0002-1517-1983
Alexander A. Makarov http://orcid.org/0000-0001-6220-6969
Alexey P. Galkin http://orcid.org/0000-0002-7362-8857

References

[1] Dreyfuss G, Kim VN, Kataoka N. Messenger-RNA-binding proteins and the messages they carry. Nat Rev Mol Cell Biol. 2002;3(3):195–205. doi: 10.1038/nrm760

[2] Ripin N, Parker R. Formation, function, and pathology of RNP granules. Cell. 2023;186(22):4737–4756. doi: 10.1016/j.cell.2023.09.006

[3] Müller-McNicoll M, Neugebauer KM. How cells get the message: dynamic assembly and function of mRNA-protein complexes. Nat Rev Genet. 2013;14 (4):275–287. doi: 10.1038/nrg3434

[4] Lunde BM, Moore C, Varani G. RNA-binding proteins: modular design for efficient function. Nat Rev Mol Cell Biol. 2007;8(6):479–490. doi: 10.1038/nrm2178

[5] Linder P, Jankowsky E. From unwinding to clamping - the DEAD box RNA helicase family. Nat Rev Mol Cell Biol. 2011;12(8):505–516. doi: 10.1038/nrm3154

[6] Hentze MW, Castello A, Schwarzl T, et al. A brave new world of RNA-binding proteins. Nat Rev Mol Cell Biol. 2018;19(5):327–341. doi: 10.1038/nrm.2017.130

[7] Mohibi S, Chen X, Zhang J. Cancer the'RBP'eutics-RNA-binding proteins as therapeutic targets for cancer. Pharmacol Ther. 2019;203:107390. doi: 10.1016/j.pharmthera.2019.07.001

[8] Mueller S, Decker L, Menge S, et al. The fragile X protein family in amyotrophic lateral sclerosis. Mol Neurobiol. 2023;60(7):3898–3910. doi: 10.1007/s12035-023-03330-x

[9] Siomi MC, Siomi H, Sauer WH, et al. FXR1, an autosomal homolog of the fragile X mental retardation gene. EMBO J. 1995;14(11):2401–2408. doi: 10.1002/j.1460-2075.1995.tb07237.x

[10] Siomi MC, Zhang Y, Siomi H, et al. Specific sequences in the fragile X syndrome protein FMR1 and the FXR proteins mediate their binding to 60S ribosomal subunits and the interactions among them. Mol Cell Biol. 1996;16(7):3825–3832. doi: 10.1128/MCB.16.7.3825

[11] Myrick LK, Hashimoto H, Cheng X, et al. Human FMRP contains an integral tandem Agenet (Tudor) and KH motif in the amino terminal domain. Hum Mol Genet. 2015;24(6):1733–1740. doi: 10.1093/hmg/ddu586

[12] Xu XL, Zong R, Li Z, et al. FXR1P but not FMRP regulates the levels of mammalian brain-specific microRNA-9 and microRNA-124. J Neurosci. 2011;31(39):13705–13709. doi: 10.1523/JNEUROSCI.2827-11.2011

[13] Agote-Arán A, Lin J, Sumara I. Fragile X-Related Protein 1 Regulates Nucleoporin Localization in a Cell Cycle-Dependent Manner. Front Cell Dev Biol. 2021;9:755847. doi: 10.3389/fcell.2021.755847

[14] Herman AB, Vrakas CN, Ray M, et al. FXR1 Is an IL-19-Responsive RNA-Binding Protein that Destabilizes Pro-inflammatory Transcripts in Vascular Smooth Muscle Cells. Cell Rep. 2018;24(5):1176–1189. doi: 10.1016/j.celrep.2018.07.002

[15] George J, Li Y, Kadamberi IP, et al. RNA-binding protein FXR1 drives cMYC translation by recruiting eIF4F complex to the translation start site. Cell Rep. 2021;37(5):109934. doi: 10.1016/j.celrep.2021.109934

[16] Tran SS, Jun HI, Bahn JH, et al. Widespread RNA editing dysregulation in brains from autistic individuals. Nat Neurosci. 2019;22(1):25–36. doi: 10.1038/s41593-018-0287-x

[17] Majumder M, Johnson RH, Palanisamy V. Fragile X-related protein family: a double-edged sword in neurodevelopmental disorders and cancer. Crit Rev Biochem Mol Biol. 2020;55(5):409–424. doi: 10.1080/10409238.2020.1810621

[18] Kirkpatrick LL, KA M, Nelson DL. Comparative genomic sequence analysis of the FXR gene family: FMR1, FXR1, and FXR2. Genomics. 2001;78(3):169–177. doi: 10.1006/geno.2001.6667

[19] Coy JF, Sedlacek Z, Bächner D, et al. Highly conserved 3' UTR and expression pattern of FXR1 points to a divergent gene regulation of FXR1 and FMR1. Hum Mol Genet. 1995;4(12):2209–2218. doi: 10.1093/hmg/4.12.2209

[20] Devys D, Lutz Y, Rouyer N, et al. The FMR-1 protein is cytoplasmic, most abundant in neurons and appears normal in carriers of a fragile X premutation. Nat Genet. 1993;4(4):335–340. doi: 10.1038/ng0893-335

[21] Khandjian EW, Fortin A, Thibodeau A, et al. A heterogeneous set of FMR1 proteins is widely distributed in mouse tissues and is modulated in cell culture. Hum Mol Genet. 1995;4(5):783–789. doi: 10.1093/hmg/4.5.783

[22] Tamanini F, Willemsen R, van Unen L, et al. Differential expression of FMR1, FXR1 and FXR2 proteins in human brain and testis. Hum Mol Genet. 1997;6(8):1315–1322. doi: 10.1093/hmg/6.8.1315

[23] Winograd C, Ceman S. Fragile X family members have important and non-overlapping functions. Biomol Concepts. 2011;2(5):343–352. doi: 10.1515/BMC.2011.033

[24] Garnon J, Lachance C, Di Marco S, et al. Fragile X-related protein FXR1P regulates proinflammatory cytokine tumor necrosis factor expression at the post-transcriptional level. J Biol Chem. 2005;280 (7):5750–5763. doi: 10.1074/jbc.M401988200

[25] Markmiller S, Soltanieh S, Server KL, et al. Context-Dependent and Disease-Specific Diversity in Protein Interactions within Stress Granules. Cell. 2018;172 (3):590–604.e13. doi: 10.1016/j.cell.2017.12.032

[26] Glauninger H, Wong Hickernell CJ, Bard JAM, et al. Stressful steps: Progress and challenges in understanding stress-induced mRNA condensation and accumulation in stress granules. Mol Cell. 2022;82 (14):2544–2556. doi: 10.1016/j.molcel.2022.05.014

[27] Hofmann S, Kedersha N, Anderson P, et al. Molecular mechanisms of stress granule assembly and disassembly. Biochim Biophys Acta Mol Cell Res. 2021;1868(1):118876. doi: 10.1016/j.bbamcr.2020.118876

[28] Marcelo A, Koppenol R, de Almeida LP, et al. Stress granules, RNA-binding proteins and polyglutamine diseases: too much aggregation? Cell Death Dis. 2021;12(6):592. doi: 10.1038/s41419-021-03873-8

[29] Aulas A, Fay MM, Lyons SM, et al. Stress-specific differences in assembly and composition of stress granules and related foci. J Cell Sci. 2017;130(5):927–937. doi: 10.1242/jcs.199240

[30] Martin JL, Dawson SJ, Gale JE. An emerging role for stress granules in neurodegenerative disease and hearing loss. Hear Res. 2022;426:108634. doi: 10.1016/j.heares.2022.108634

[31] Younas N, Zafar S, Shafiq M, et al. SFPQ and Tau: critical factors contributing to rapid progression of Alzheimer's disease. Acta Neuropathol. 2020;140 (3):317–339. doi: 10.1007/s00401-020-02178-y

[32] Strohmeyer R, Rogers J. Molecular and cellular mediators of Alzheimer's disease inflammation. J Alzheimer's disease: JAD. 2001;3(1):131–157. doi: 10.3233/jad-2001-3118

[33] Sopova JV, Koshel EI, Belashova TA, et al. RNA-binding protein FXR1 is presented in rat brain in amyloid form. Sci Rep. 2019;9(1):18983. doi: 10.1038/s41598-019-55528-6

[34] Velizhanina ME, Galkin AP. Amyloid Properties of the FXR1 Protein Are Conserved in Evolution of Vertebrates. Int J Mol Sci. 2022;23(14):7997. doi: 10.3390/ijms23147997

[35] Mazroui R, Huot ME, Tremblay S, et al. Trapping of messenger RNA by Fragile X Mental Retardation protein into cytoplasmic granules induces translation repression. Hum Mol Genet. 2002;11(24):3007–3017. doi: 10.1093/hmg/11.24.3007

[36] Hofmann I, Casella M, Schnölzer M, et al. Identification of the junctional plaque protein plakophilin 3 in cytoplasmic particles containing RNA-binding proteins and the recruitment of plakophilins 1 and 3 to stress granules. Mol Biol Cell. 2006;17(3):1388–1398. doi: 10.1091/mbc.e05-08-0708

[37] Mazroui R, Sukarieh R, Bordeleau ME, et al. Inhibition of ribosome recruitment induces stress granule formation independently of eukaryotic initiation factor 2alpha phosphorylation. Mol Biol Cell. 2006;17(10):4212–4219. doi: 10.1091/mbc.e06-04-0318

[38] Kayed R, Head E, Sarsoza F, et al. Fibril specific, conformation dependent antibodies recognize a generic epitope common to amyloid fibrils and fibrillar oligomers that is absent in prefibrillar oligomers. Mol Neurodegener. 2007;2(1):18. doi: 10.1186/1750-1326-2-18

[39] Wolozin B, Ivanov P. Stress granules and neurodegeneration. Nat Rev Neurosci. 2019;20(11):649–666. doi: 10.1038/s41583-019-0222-5

[40] Rubel AA, Ryzhova TA, Antonets KS, et al. Identification of PrP sequences essential for the interaction between the PrP polymers and Aβ peptide in a yeast-based assay. Prion. 2013;7(6):469–476. doi: 10.4161/pri.26867

[41] Laurén J, Gimbel DA, Nygaard HB, et al. Cellular prion protein mediates impairment of synaptic plasticity by amyloid-beta oligomers. Nature. 2009;457(7233):1128–1132. doi: 10.1038/nature07761

[42] Gauczynski S, Peyrin JM, Haïk S, et al. The 37-kDa/67-kDa laminin receptor acts as the cell-surface receptor for the cellular prion protein. EMBO J. 2001;20(21):5863–5875. doi: 10.1093/emboj/20.21.5863

[43] Younas N, Zafar S, Saleem T, et al. Differential interactome mapping of aggregation prone/prion-like proteins under stress: novel links to stress granule biology. Cell Biosci. 2023;13(1):221. doi: 10.1186/s13578-023-01164-7

[44] Karpova TS, Baumann CT, He L, et al. Fluorescence resonance energy transfer from cyan to yellow fluorescent protein detected by acceptor photobleaching using confocal microscopy and a single laser. J Microsc. 2003;209(Pt 1):56–70. doi: 10.1046/j.1365-2818.2003.01100.x

[45] Ishikawa-Ankerhold HC, Ankerhold R, Drummen GP. Advanced fluorescence microscopy techniques–FRAP, FLIP, FLAP, FRET and FLIM. Molecules. 2012;17(4):4047–4132. doi: 10.3390/molecules17044047

[46] Hughes MP, Sawaya MR, Boyer DR, et al. Atomic structures of low-complexity protein segments reveal kinked β sheets that assemble networks. Science. 2018;359(6376):698–701. doi: 10.1126/science.aan6398

[47] Luo F, Gui X, Zhou H, et al. Atomic structures of FUS LC domain segments reveal bases for reversible amyloid fibril formation. Nat Struct Mol Biol. 2018;25(4):341–346. doi: 10.1038/s41594-018-0050-8

[48] Gui X, Luo F, Li Y, et al. Structural basis for reversible amyloids of hnRNPA1 elucidates their role in stress granule assembly. Nat Commun. 2019;10(1):2006. doi: 10.1038/s41467-019-09902-7

[49] Guenther EL, Cao Q, Trinh H, et al. Atomic structures of TDP-43 LCD segments and insights into reversible or pathogenic aggregation. Nat Struct Mol Biol. 2018;25(6):463–471. doi: 10.1038/s41594-018-0064-2

[50] Sekiyama N, Takaba K, Maki-Yonekura S, et al. ALS mutations in the TIA-1 prion-like domain trigger highly condensed pathogenic structures. Proc Natl Acad Sci USA. 2022;119(38):e2122523119. doi: 10.1073/pnas.2122523119

[51] Mason TO, Shimanovich U. Fibrous Protein Self-Assembly in Biomimetic Materials. Adv Mater. 2018;30(41):e1706462. doi: 10.1002/adma.201706462

[52] Lee M, Sadowska A, Bekere I, et al. The structure of human SFPQ reveals a coiled-coil mediated polymer essential for functional aggregation in gene regulation. Nucleic Acids Res. 2015;43(7):3826–3840. doi: 10.1093/nar/gkv156

[53] Antonets KS, Sargsyan HM, Nizhnikov AA. A Glutamine/Asparagine-Rich Fragment of Gln3, but not the Full-Length Protein, Aggregates in Saccharomyces cerevisiae. Biochemistry (Mosc). 2016;81(4):407–413. doi: 10.1134/S0006297916040118

[54] Gietz RD, Schiestl RH. High-efficiency yeast transformation using the LiAc/SS carrier DNA/PEG method. Nat Protoc. 2007;2(1):31–34. doi: 10.1038/nprot.2007.13

[55] Kachkin DV, Lashkul G VV, NA, et al. The Aβ42 Peptide and IAPP Physically Interact in a Yeast-Based Assay. Int J Mol Sci. 2023;24(18):14122. doi: 10.3390/ijms241814122

[56] Sergeeva AV, Sopova JV, Belashova TA, et al. Amyloid properties of the yeast cell wall protein Toh1 and its interaction with prion proteins Rnq1 and Sup35. Prion. 2019;13(1):21–32. doi: 10.1080/19336896.2018.1558763